Fuel Cells

DOI: 10.1002/ange.200700411

Computational Study on the Catalytic Mechanism of Oxygen Reduction on $La_{0.5}Sr_{0.5}MnO_3$ in Solid Oxide Fuel Cells**

*YongMan Choi, M. C. Lin, and Meilin Liu**

Dedicated to Süd-Chemie on the occasion of its 150th anniversary

The development of novel cathode materials for solid oxide fuel cells (SOFCs) that operate at intermediate temperatures (500–700 °C) has attracted much attention[1] because of their potential to dramatically reduce the cost of SOFC technology.[2] Strontium-doped lanthanum manganite $La_{1-x}Sr_xMnO_{3-\delta}$ (LSM) has been widely used as a cathode for SOFCs because of its excellent thermal and chemical compatibility with the YSZ electrolyte (yttria-stabilized zirconia; 8 mol% Y_2O_3). However, its catalytic activity is inadequate for low-temperature applications.[3] To date, several types of perovskite cathode materials have been studied to replace LSM but with little success; they include Sr-doped lanthanum cobaltite ($La_{1-x}Sr_xCoO_{3-\delta}$, LSC) with high oxygen-ion conductivity.

In order to design new cathode materials for SOFCs, one must understand the detailed mechanism of oxygen reduction. Numerous phenomenological studies[4] suggest that oxygen reduction at the surface of a mixed ionic–electronic conductor (MIEC) cathode (e.g., LSM and LSC) consists of many elementary steps, which include adsorption of a superoxo- or peroxo-like species (O_2^- or O_2^{2-}, respectively), dissociation of diatomic oxygen to monoatomic oxygen, and incorporation of oxygen species into the bulk lattice. Similar oxygen reduction processes occur at a triple-phase boundary (TPB), where a cathode, an electrolyte, and oxygen species meet. Recently, it was predicted that oxygen reduction on undoped $LaMnO_3$ may occur with small reaction barriers or without barrier via superoxo- or peroxo-like intermediates.[5] Although several theoretical investigations on pure or Sr-doped $LaMnO_3$ have been reported,[6–8] detailed mechanistic studies of oxygen reduction on the surfaces of a Sr-doped $LaMnO_3$ cathode by means of quantum chemical calculations are still lacking. Here we report our findings in applying ab initio methods using periodic density functional theory (DFT) to predict the interactions between oxygen species and $La_{0.5}Sr_{0.5}MnO_3$ surfaces. Molecular dynamics (MD) calculations were performed to simulate SOFC operating conditions at 1073 K. This understanding is vital for the rational design of novel cathode materials for SOFCs.

As shown in Figure 1, in order to construct Sr-doped $LaMnO_3$ surfaces ($La_{0.5}Sr_{0.5}MnO_3$), we applied LaMnO-terminated $LaMnO_3$ (110) among (111), (110), and (100), because the (110) surface includes all A, B, O ions of perovskite-structure ABO_3 cathode materials, and thus allows examination of the activity of both A and B cations. Regarding interactions of $LaMnO_3$ (110) and O_2, it was found that the O-terminated surface is energetically less favorable than the LaMnO-terminated surface (Figure 1 g).[5] Thus, in this study, the LaMnO-terminated (110) surface was used to obtain $La_{0.5}Sr_{0.5}MnO_3$ surface models by replacing 50% of the La^{3+} ions with divalent Sr^{2+} ions. Substitution of each La^{3+} by Sr^{2+} produces a half doubly charged oxygen vacancy,[9] as described by the defect reaction (1) (Kröger–Vink notation).

$$2\,SrO + 2\,La_{La}^{x} + O_O^x \rightarrow 2\,Sr'_{La} + V_O^{\cdot\cdot} + La_2O_3 \qquad (1)$$

Here, La_{La}^{x}, O_O^x, Sr'_{La}, and $V_O^{\cdot\cdot}$ denote an La cation at a regular La site, an oxygen ion at a regular oxygen site, a Sr cation at an La site with one effective negative charge, and an oxygen vacancy with two effective positive charges, respectively. As shown in Figure 1, we assume that an oxygen vacancy is located on the top layer to examine the effect of oxygen vacancy on O_2–LSM interactions, which leads to six possible surface models. Table 1 compiles calculated oxygen-vacancy formation energies and lattice constants for the six $La_{0.5}Sr_{0.5}MnO_3$ surface models. The predicted lattice constants

[*] Dr. Y. Choi, Prof. M. Liu
Center for Innovative Fuel Cell and Battery Technologies
School of Materials Science and Engineering
Georgia Institute of Technology
Atlanta, GA 30332 (USA)
Fax: (+1) 404-894-9140
E-mail: yongman.choi@mse.gatech.edu
meilin.liu@mse.gatech.edu
Prof. M. C. Lin
Department of Chemistry
Emory University
1515 Dickey Drive, Atlanta, GA 30322 (USA)
Fax: (+1) 404-727-6586
E-mail: chemmcl@emory.edu
and
Center for Interdisciplinary Molecular Science
National Chiao Tung University
Hsinchu, 30010 (Taiwan)
Fax: (+886) 3-571-2179

[**] This work was supported by the U.S. DOE Basic Energy Science (under Grant No. DE-FG02-06ER15837DOE) and the University Coal Program (under Grant No. DEFG26-06NT42735). The authors acknowledge the use of CPUs from National Center for High-Performance Computing, Taiwan, supported by INER under contract No. NL 940251. M.C.L. also acknowledges supports from the MOE ATP program, Taiwan Semiconductor Manufacturing Co. for the TSMC Distinguished Professorship and Taiwan National Science Council for the Distinguished Visiting Professorship at the Center for Interdisciplinary Molecular Science, National Chiao Tung University, Hsinchu, Taiwan. Y.M.C. thanks Dr. Daniel Spišák for drawing of charge density differences.

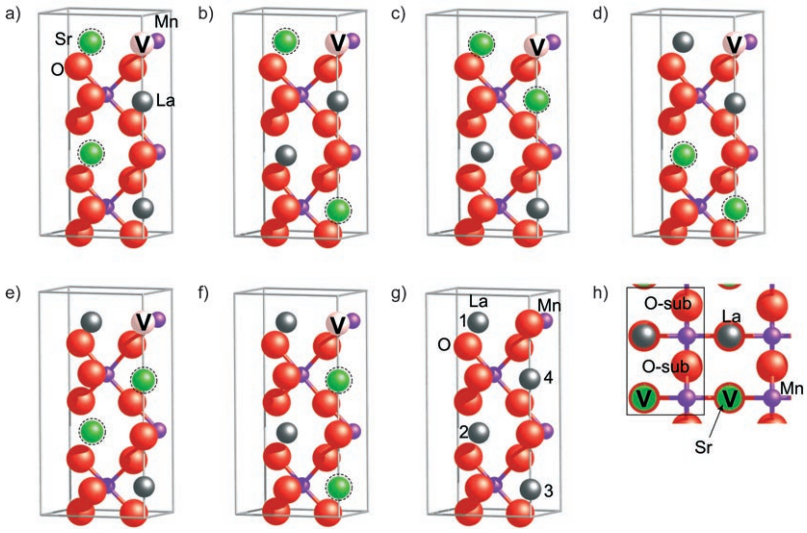

Figure 1. a)–f) $La_{0.5}Sr_{0.5}MnO_3$(110) surface models (**A**, **B**, **C**, **D**, **E**, and **F**, respectively) and g) undoped $LaMnO_3$(110). Dashed circles and **V** denote Sr cations and doubly charged oxygen vacancies, respectively. h) Top view of adsorption sites on LaMn-terminated $La_{0.5}Sr_{0.5}MnO_3$ (110) (surface model **F**). The rectangle represents a supercell for surface calculations; it contains a total of 19 ions (two La, two Sr, four Mn, and 11 O ions) and an oxygen vacancy. La gray, Sr green, Mn purple, O red.

Table 1: Calculated energies for oxygen-vacancy formation and lattice constants of LaMn-terminated $La_{0.5}Sr_{0.5}MnO_3$(110) surface models shown in Figure 1.

Surface model	Oxygen-vacancy formation energy [eV]	Lattice constant [Å]
A	8.10	3.804
B	8.12	3.812
C	8.12	3.812
D	8.20	3.799
E	8.17	3.791
F	8.13	3.797

are only slightly different from that of $LaMnO_3$ (3.876 Å).[5] Also, among these models, the differences in oxygen-vacancy formation energies and lattice constants are insignificant. We chose surface model **F** (Figure 1 f) for subsequent studies of O_2–LSM interactions due to the presence of the La cation in the first layer and because it has a lower oxygen-vacancy formation energy than surface models **D** and **E**. For brevity, we use LSM0.5 to denote LaMn-terminated $La_{0.5}Sr_{0.5}MnO_3$-(110) as shown in Figure 1 f. Further, Evarestov and co-workers[8] reported that the effect of asymmetric and symmetric $LaMnO_3$(110) surface models on surface energies is negligible.[10] Accordingly, the effect of dipole moment on oxygen reduction was neglected in this study, although the (110) surface is polar.

We investigated O_2 adsorption on LSM0.5 at a coverage of 0.5 monolayers (ML) by placing an oxygen molecule on each cation site, as depicted in Figure 1 h. A coverage of 0.5 ML implies that one oxygen species is adsorbed on one of the two cations on the top layer. As summarized in Table 2, we initially determined molecularly adsorbed precursors, which could be used as an initial or final state for minimum-energy path (MEP) calculations using the nudged elastic band (NEB) method.[11] Figure 2 shows geometrical representations of optimized oxygen species on LSM0.5. The predicted O–O distance and vibrational frequency of triplet O_2 (1.235 Å and 1558 cm^{-1}, respectively) in a 10-Å cubic box are in good agreement with experimental results (1.207 Å[12] and 1550 cm^{-1},[13] respectively).

Table 2 lists adsorption energies, bond lengths, and vibrational frequencies of oxygen species adsorbed on the La and Mn cations. Adsorption of molecular oxygen at the Mn cation on LSM0.5 involves stronger bonds than that on defective $LaMnO_3$ (–1.82 eV),[5] and this implies that Sr doping influences oxygen reduction on cathode surfaces. According to the predicted bond length, configuration, and vibrational frequency of the molecularly adsorbed intermediate species, we classified them as superoxo- or peroxo-like species (Table 2). In particular, a 2×2 enlarged surface in x and y directions was

Table 2: Adsorption energies, bond lengths, and vibrational frequencies of adsorbed oxygen species on LSM0.5.

Species	ΔE [eV]	r(O–O) [Å]	r(O–M) [Å]	$\tilde{\nu}_{OO}$ [cm^{-1}]	Remark
$LSM0.5 + O_2$	0.00	–	–	–	–
O_2	–	1.235	–	1558	–
La-super	–1.10	1.299	2.271	1218	superoxo
La-diss	–5.20	–	1.908	–	–
Mn-super	–1.93	1.319	1.742	1182	superoxo
Mn-per	–2.79	1.426	1.842	909	peroxo
			1.841		
Mn-diss	–6.69	–	1.653	–	–
Mn-diff[a]	–8.47	–	–	–	–

[a] Final product in the mechanistic study.

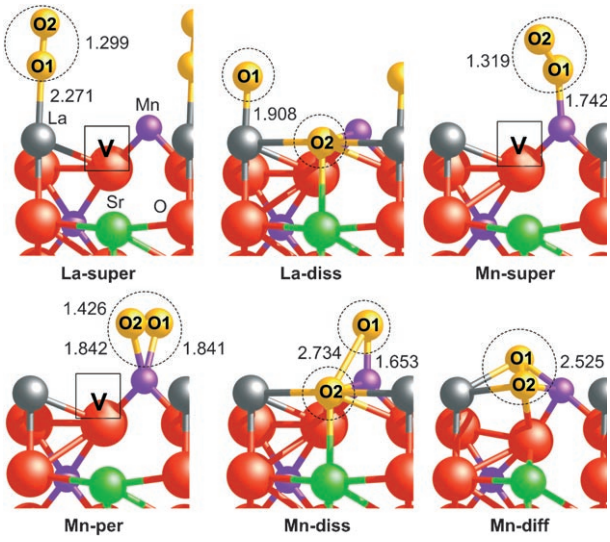

Figure 2. Structural representation of optimized oxygen species on LSM0.5 via molecular adsorption. The species in dashed circles are adsorbed oxygen species. **V** denotes an oxygen vacancy.

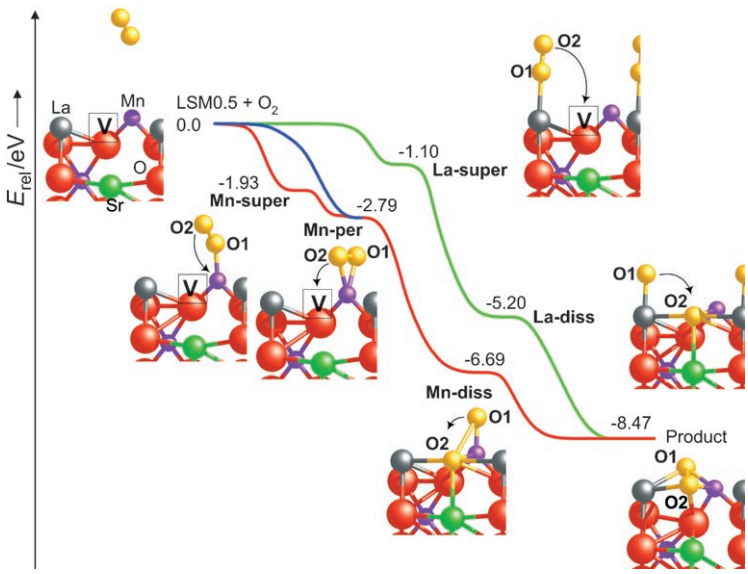

Figure 3. Energy profiles illustrating oxygen reduction on LSM0.5.

constructed to compare effects of coverage on the O_2–LSM0.5 interactions based on the **Mn-super** configuration. Adsorption energies per O_2 at a coverage of 0.5 ML on the two surface models are similar (−1.93 vs −1.87 eV). Accordingly, we assumed that the surface size of LSM0.5 shown in Figure 1 may be sufficient for characterizing the oxygen reduction reaction.

To carry out mechanistic studies on the oxygen reduction on LSM0.5, potential-energy profiles were constructed by mapping out MEPs by using the NEB method.[11] The molecularly adsorbed or dissociated oxygen species on the LSM0.5 surface were connected by the NEB method as shown in Figure 3. The potential-energy profiles displayed in Figure 3 indicate that molecular adsorption on La and Mn cations with superoxo-like characteristics occur without well-defined transition states similar to those on $LaMnO_3$ surfaces.[5] The process, predicted to be exothermic by 1.10 and 1.93 eV, respectively, occurs smoothly along the MEP by lengthening of the **O1**–**O2** bond and shortening of the **O1**–M (M = La or Mn) bond (from 1.299 to 1.319 Å and from 2.271 to 1.742 Å, respectively). Adsorption on the Mn cation is more stable than that on the La cation. While the **Mn-per** intermediate with peroxo-like characteristics can form directly from the reactants without a well-defined transition state, we were unable to locate a peroxo-like species via adsorption on the La cation. For the pathway via the **La-super** intermediate, due to the nonexistence of the peroxo-like species, the intermediate directly dissociates and is incorporated into the bulk phase to produce **La-diss** with an exothermicity of 5.20 eV (Figure 3). Our extensive search to locate a transition state between **Mn-super** and **Mn-per** confirmed that this transformation takes place barrierlessly. The formation of **Mn-per** is exothermic by 2.79 eV and the intermediate can decompose barrierlessly to give **Mn-diss**. The monatomic oxygen species (**O1**) adsorbed on a surface La ion (**La-diss**) and that adsorbed on a surface Mn ion (**Mn-diss**) diffuses to a more energetically stable site (**Mn-diff**, labeled as Product in Figure 3) that lies 8.47 eV below the reactants. It is thus expected that the dissociated oxygen species (**O1** and **O2**) are involved in oxygen-ion transport in the bulk phase or diffuse to the TPB, the electrochemically active site. The MEP calculations suggest that the overall process may take place very fast because no reaction barriers are involved.

Figure 4 illustrates an increase in charge density as a gas-phase O_2 molecule is adsorbed on LSM0.5 via the Mn cation pathway. Due to charge transfer from the surface, especially from La and Mn cations in the first layer, to the oxygen species (π_g^* states; see the change in Figure 4), the O–O bond weakens. Compared to that of the reactant O_2 with 1.235 Å, those of **La-super** and **Mn-super** are elongated by approximately 5 and 7%, respectively (Figure 2). The effective charges calculated by means of the Bader analysis program[14] also clearly demonstrate charge transfer between the adsorbates and the substrate. The charge becomes more negative as the adsorption/dissociation proceeds. The O–Mn chemical bonding of **Mn-super** involves 0.51 electrons. The 0.42 electrons involved in the O–La bonding of **La-super** imply a

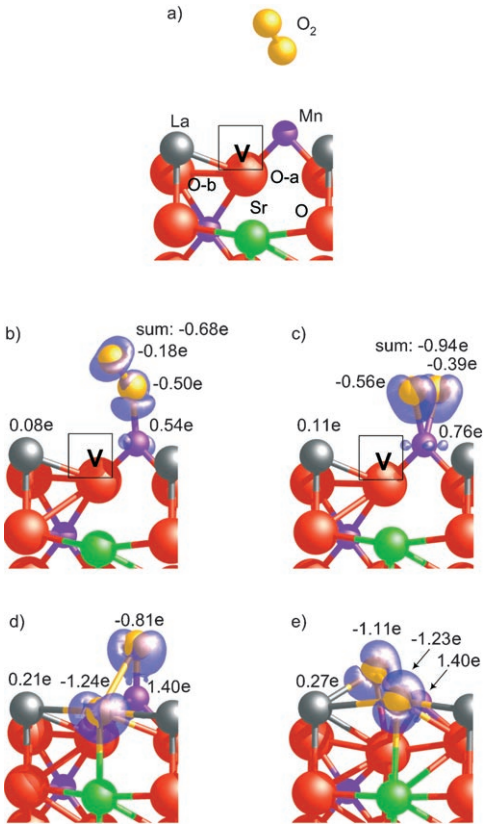

Figure 4. Illustration of charge-density changes in oxygen reduction on LSM0.5 via the Mn-cation pathway. a) Before interaction, b) adsorbed superoxo-like **Mn-super**, c) adsorbed peroxo-like **Mn-per**, d) after dissociation/incorporation into the bulk phase, **Mn-diss**, and e) diffusion on the surface, **Mn-diff**. $\Delta\rho_{diff}$ isosurfaces were calculated at 0.00012 e Å^3. The values are effective charges relative to those of the reactants.

weaker bond than that of **Mn-super**. Further charge transfer occurs as the molecularly adsorbed **Mn-per** species dissociates and is incorporated into the oxygen vacancy (1.24 electrons for **Mn-diss**). Only 0.51 electron of **Mn-super** transferred from LSM0.5 are involved in the interaction, whereas the 0.94 electrons of **Mn-per** that participate in bond formation lead to stronger adsorption (−1.93 vs −2.79 eV). After incorporation into the lattice, charge transfer is accelerated, leading to a similar effective charge of $-1.24\,|e|$ to those of the bulk oxygen anions of O-a and O-b (-1.30 and $-1.29\,|e|$, respectively; see Figure 4). After the atomic oxygen species adsorbed on the Mn cation (**Mn-diss**) moves to a more stable site (e.g., near the O-a site), its effective charge becomes more negative (from -0.81 to $-1.11\,|e|$) due to interaction with the La cation of the top layer.

Furthermore, the oxygen reduction reaction was examined by local densities of states (LDOS) calculations for the adsorbed oxygen species on the Mn cation, as well as the La and Mn cations on the top layer. Figure 5a shows the LDOS

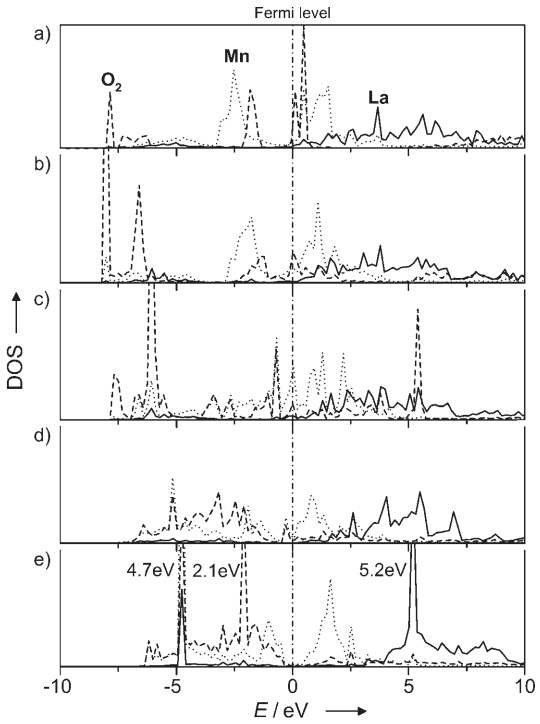

Figure 5. Local density of states for oxygen reduction on LSM0.5 via the Mn-cation pathway. a) Before interaction, b) **Mn-super**, c) **Mn-per**, d) **Mn-diss**, and e) **Mn-diff**. Dashed lines: O_2 p; solid lines: La 5d; dotted lines: Mn 5d.

before O_2–LSM0.5 interactions. Figures 5b and c correspond to the LDOS after adsorption with superoxo- and peroxo-like configurations (**Mn-super** and **Mn-per**, respectively) and clearly shows strong hybridization of O p and Mn 5d. As the interactions proceed, the gap below the Fermi level in Figure 5a gradually decreases due to hybridization of pd states of adsorbed oxygen species and the La and Mn cations. As displayed in Figure 5d, after dissociation/incorporation of an adsorbed oxygen species into the oxygen vacancy, more pronounced broadening occurs. In particular, due to diffusion of the adsorbed atomic oxygen on the Mn cation of **Mn-diff**, the oxygen species has similar electronic characteristics to oxygen ions in the second layer (see O-a and O-b in Figure 4a) at 2.1 and 4.7 eV below the Fermi level, and the La cation shows hybridization at 4.7 and 5.2 eV below and above the Fermi level.

We also carried out ab initio MD calculations for interactions of O_2 with LSM0.5 at 1073 K (Figure 6). The distance between the O_2 molecule and LSM0.5 was initially

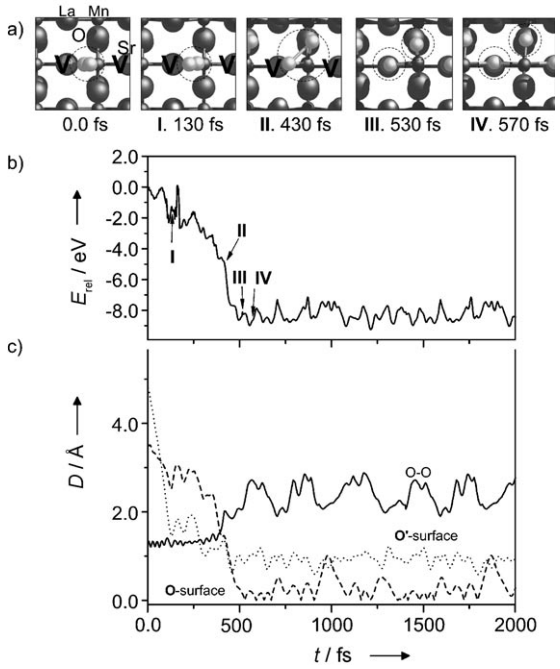

Figure 6. a) Top views of snapshots, b) an energy profile, and c) O–O and O–surface distances from MD simulations of oxygen reduction on LSM0.5 at 1073 K. **V** denotes a doubly charged oxygen vacancy. **I**, **II**, **III**, and **IV** correspond to adsorption with a superoxo-like species, conversion to a peroxo-like species, dissociation and incorporation into the bulk, and diffusion on the surface, respectively. The solid line denotes the O–O distance. Dashed and dotted lines are the shortest distances between **O** and **O′** and the surface, respectively.

set at about 4.8 Å with a configuration similar to that of **Mn-super** shown in Figure 2, and it was fully optimized as representing a nonbonded O_2 molecule and clean LSM0.5. A time step of 2 fs and the Nosé–Hoover thermostat[15] were employed. Figure 6a displays top views of snapshots of significant states during the MD simulations. Figure 6b and 6c illustrate the variation of relative energies, the O–O bond length, and the distances of **O** and **O′** from the surface as a function of time. As the free O_2 molecule is first adsorbed at the Mn ion, the energy gradually decreases. During the course of the initial adsorption process, rotation of O_2 produces a hill at about 80 fs in the energy profile and crossing of the **O**– and **O′**–surface distances (Figure 6c). After about 130 fs, O_2 is reduced to form a superoxo-like species with an exothermicity of about 2.0 eV (see the end-on structure in Figure 6a). The O–O distance slightly increases compared to that of the

reactant O_2. However, the O–O bond elongates remarkably after about 350 fs (1.46 Å), along with overcoming some barriers (i.e., at ca. 165 fs) and more reduction. At about 430 fs, the superoxo-like species is fully converted to a peroxo-like species parallel to the surface, which leads to overlap of the **O**– and **O′**–surface distances (see Figure 6c). After reduction from the superoxo- to the peroxo-like species, one of the oxygen atoms of the peroxo-like configuration is incorporated into the bulk phase (an oxygen vacancy) at about 530 fs, followed by surface diffusion of the other oxygen atom to a more stable site at about 570 fs. The MD simulations reach an equilibrium state with oscillation of the O–O distance (2.38 ± 0.27 Å). The whole process is completed with a highly exothermic energy of about 8.5 eV that implies fast O_2 kinetics. The energy profile from the MD simulations indicates superoxo- and peroxo-like species have very short lifetimes. In addition, MD simulations in conjunction with NEB calculations clearly show that oxygen reduction on LSM0.5 occurs by a stepwise reaction mechanism. The oxygen species then diffuse into the lattice.

In summary, DFT and MD calculations for oxygen reduction on a $La_{0.5}Sr_{0.5}MnO_3$(110) surface suggest that O_2 species are preferentially adsorbed on the Mn site rather than the La site according to the difference in adsorption energy, which supports the fact that B cations are more active than A cations for oxygen reduction on several perovskite-type ABO_3 cathodes. The combination of MEP and MD calculations suggested a fast stepwise reaction on LSM0.5, along with charge transfer from the surface to the adsorbed oxygen species. The nonexistence of intrinsic transition-state barriers results in fast O_2 reduction on LSM-based cathodes in SOFCs. Furthermore, the high adsorption energies of 1.93 and 2.79 eV on the Mn site compared to those on metal surfaces[16]—the most stable O_2 intermediates on Pt, Ni, Pd, Cu, and Ir(111) have adsorption energies of 0.72, 1.67, 1.01, 0.56, and 1.27 eV, respectively—imply that LSM-based cathode materials are more efficient for O_2 adsorption. This information about reaction mechanism, catalytic activity of different surface sites, as well as their dependence on surface structure and defects (e.g., oxygen vacancy) would be otherwise difficult to obtain (i.e., by experimental measurements), implying that quantum chemical calculations could play a vital role in rational design of better electrode materials for SOFCs.

Computational Section

All calculations were carried out by periodic density function theory (DFT) with the projector-augmented wave (PAW)[17] method, as implemented in the Vienna ab initio simulation package (VASP).[18] The generalized gradient approximation (GGA) with the Perdew–Wang (PW91) exchange-correlation functional[19] was used. La, Sr, Mn, and O atoms were described by 11 ($5s^25p^65d^16s^2$), 10 ($4s^24p^65s^2$), 7 ($4s^13d^6$), and 6 ($2s^2sp^4$) valence electrons, respectively; the cutoff energies were 219.271, 226.196, 269.887, and 400.000 eV, respectively. The kinetic energy cutoff for a plane-wave basis set was 400 eV. We applied a Monkhorst–Pack mesh[20] with $(4 \times 4 \times 4)$ **k**-points, allowing convergence to 0.01 eV of the total electronic energy. Similar to the previous studies on perovskite-type materials,[7,21] only the highly symmetric structure of *Pm*3*m* was examined, because $LaMnO_3$-based cathode materials have a cubic structure under SOFC operating conditions (above 500 °C in ambient air).[8]

All calculations were performed by using the spin-polarization method to properly describe the magnetic property of the $La_{0.5}Sr_{0.5}MnO_3$ surface model and oxygen reduction: O_2 is a spin-polarized triplet in its ground state. It was found that the ferromagnetic (FM) configuration is more stable than the antiferromagnetic configuration (AFM) in the bulk structure of $La_{0.5}Sr_{0.5}MnO_3$, with a difference in energy of about 0.3 eV. Thus, we used the FM state in this study. For the 2D slab-model calculations, metal oxide surfaces comprising eight atomic layers were separated by a vacuum space equivalent of 24 Å in the direction perpendicular at the surface. Similar to our previous study,[5] all surface calculations for the interactions between molecular oxygen species and $La_{0.5}Sr_{0.5}MnO_3$ were performed by relaxing the top three layers while keeping the bottom five layers to the estimated bulk parameters. In this work, the adsorption energy was calculated according to $\Delta E = E[\text{adsorbate–adsorbent}] - E[\text{adsorbate}] - E[O_2]$, where E[adsorbate–adsorbent] and E[adsorbate] are the calculated electronic energies of bonded oxygen species on the surface and a clean surface, respectively, and $E[O_2]$ denotes the energy for triplet O_2. The change in charge density due to oxygen reduction was calculated by $\Delta\rho_{\text{diff}} = \rho[\text{adsorbate–adsorbent}] - \rho[\text{adsorbate}] - \rho[\text{adsorbent}]$. The reaction pathways of the oxygen reduction process on the $La_{0.5}Sr_{0.5}MnO_3$ surface were investigated by using the nudged elastic band (NEB) method.[11] All of our transition-state searches were performed by interpolating a series of eight images of the system between reactant and product states on potential-energy surfaces. Molecular dynamics (MD) calculations using the VASP code were performed to examine the process at 1073 K.

Received: January 30, 2007
Revised: April 6, 2007
Published online: July 18, 2007

Keywords: ab initio calculations · fuel cells · molecular dynamics · reaction mechanisms · reduction

[1] a) N. Q. Minh, T. Takahashi, *Science and Technology of Ceramic Fuel Cells*, Elsevier, Amsterdam, **1995**; b) P. Singh, N. Q. Minh, *Int. J. Appl. Ceram. Technol.* **2004**, *1*, 5; c) C. Xia, M. Liu, *Adv. Mater.* **2002**, *14*, 521.
[2] B. C. H. Steele, A. Heinzel, *Nature* **2001**, *414*, 345.
[3] R. A. De Souza, J. A. Kilner, *Solid State Ionics* **1998**, *106*, 175.
[4] a) S. Pizzini in *Fast Ion Transport in Solids* (Ed.: W. van Gool), North-Holland, **1973**, p. 461; b) B. C. H. Steele, *Solid State Ionics* **1996**, *86–88*, 1223; c) M. Liu, *J. Electrochem. Soc.* **1998**, *145*, 142; d) M. Liu, J. Winnick, *Solid State Ionics* **1999**, *118*, 11; e) S. B. Adler, *Chem. Rev.* **2004**, *104*, 4791.
[5] Y. M. Choi, D. S. Mebane, M. C. Lin, M. Liu, *Chem. Mater.* **2007**, *19*, 1690; the estimated bulk lattice constant for $LaMnO_3$ is 3.876 Å. Reaction barriers for converting superoxo- to peroxo-like species adsorbed on La and Mn sites on perfect $LaMnO_3$ are 0.01 and 0.08 eV, respectively, while that on the Mn site on a defective $LaMnO_3$ is 0.1 eV.
[6] a) W. E. Pickett, D. J. Singh, *Phys. Rev. B* **1996**, *53*, 1146; b) Y. S. Su, T. A. Kaplan, S. D. Mahanti, J. F. Harrison, *Phys. Rev. B* **2000**, *61*, 1324; c) M. Nicastro, C. H. Patterson, *Phys. Rev. B* **2002**, *65*, 205111; d) D. Muñoz, N. M. Harrison, F. Illas, *Phys. Rev. B* **2004**, *69*, 085115; e) E. A. Kotomin, R. A. Evarestov, Y. A. Mastrikov, J. Maier, *Phys. Chem. Chem. Phys.* **2005**, *7*, 2346; f) E. A. Kotomin, E. Heifets, S. Dorfman, D. Fuks, A. Gordon, J. Maier, *Surf. Sci.* **2004**, *566–568*, 231; g) E. A. Kotomin, E. Heifets, J. Maier, W. A. Goddard III, *Phys. Chem. Chem. Phys.* **2003**, *5*, 4180; h) D. Fuks, L. Bakaleinikov, E. A. Kotomin, J. Felsteiner, A. Gordon, R. A. Evarestov, D. Gryaz-

nov, J. Maier, *Solid State Ionics* **2006**, *177*, 217; i) D. Fuks, S. Dorfman, J. Felsteiner, L. Bakaleinikov, A. Gordon, E. A. Kotomin, *Solid State Ionics* **2004**, *173*, 107.

[7] a) N. N. Kovaleva, J. L. Gavartin, A. L. Shluger, A. V. Boris, A. M. Stoneham, *J. Exp. Theor. Phys.* **2002**, *94*, 178; b) R. A. Evarestov, E. A. Kotomin, D. Fuks, J. Felsteiner, J. Maier, *Appl. Surf. Sci.* **2004**, *238*, 457; c) R. A. Evarestov, E. A. Kotomin, E. Heifets, J. Maier, G. Borstel, *Solid State Commun.* **2003**, *127*, 367.

[8] R. A. Evarestov, E. A. Kotomin, Y. A. Mastrikov, D. Gryaznov, E. Heifets, J. Maier, *Phys. Rev. B* **2005**, *72*, 214411.

[9] K. S. Chan, J. Ma, S. Jaenicke, G. K. Chuah, J. Y. Lee, *Appl. Catal. A* **1994**, *107*, 201.

[10] We examined the dipole moment perpendicular to the surfaces of perfect $LaMnO_3$, defective $LaMnO_3$ with one oxygen vacancy, and $La_{0.5}Sr_{0.5}MnO_3$ with one oxygen vacancy (2.89, 2.55, and 2.53 D, respectively); the results suggest that the dipole moment of the asymmetric surface models with eight atomic layers was slightly reduced by the presence of oxygen vacancies. When seven-atomic-layer symmetric surface models terminated with O or LaMn were used, their dipole moments cancelled out (see ref. [8]).

[11] G. Henkelman, B. P. Uberuaga, H. Jönsson, *J. Chem. Phys.* **2000**, *113*, 9901.

[12] A. Bielanski, J. Haber, *Oxygen in Catalysis*, Marcel Dekker, New York, **1991**.

[13] G. Herzberg, *Molecular Spectra and Molecular Structure*, *Vol. I*, 2nd ed., Krieger Publishing Company, Malabar, FL, **1950**.

[14] a) G. Henkelman, A. Arnaldsson, H. Jönsson, *Comput. Mater. Sci.* **2006**, *36*, 354; b) http://theory.cm.utexas.edu/bader/.

[15] S. Nosé, *Mol. Phys.* **1984**, *52*, 255.

[16] Y. Xu, M. Mavrikakis, *J. Chem. Phys.* **2004**, *126*, 10846.

[17] P. E. Blöchl, *Phys. Rev. B* **1994**, *50*, 17953.

[18] a) G. Kresse, J. Furthmüller, *Phys. Rev. B* **1996**, *54*, 11169; b) G. Kresse, J. Hafner, *Phys. Rev. B* **1993**, *47*, 558.

[19] J. P. Perdew, K. Burke, M. Ernzerhof, *Phys. Rev. Lett.* **1996**, *77*, 3865.

[20] H. J. Monkhorst, J. D. Pack, *Phys. Rev. B* **1976**, *13*, 5188.

[21] P. Ravindran, A. Kjekshus, H. Fjellvag, A. Delin, O. Eriksson, *Phys. Rev. B* **2002**, *65*, 064445.

